CHAPTER IV
RESULTS AND DISCUSSION

4.1 Catalyst Characterization

4.1.1 Thermal Gravimetric Analysis (TGA)

Thermogravimetric-differential thermal analyzer (TG-DTA) was used to evaluate the suitable calcination temperature of prepared catalysts. Figure 4.1 shows TGA profiles of the catalysts. The weight loss at 100-120 °C, corresponding to desorbed water was observed on all catalysts. The weight losses at higher temperature represented the decomposition of metal precursors. The highest decomposition temperatures over Pd, Pt, Cu, NiCu, NiMo, and CoMo catalysts are 343, 230, 316, 284, 232 and 220 °C, respectively. According to TGA profiles, the suitable calcination temperatures for each catalyst were list in Table 4.1. All catalysts, except Pt catalyst, were calcined at 500 °C. Pt catalyst was calcined at 350 °C, since the weight loss of Pt precursor was quite low after 350 °C.

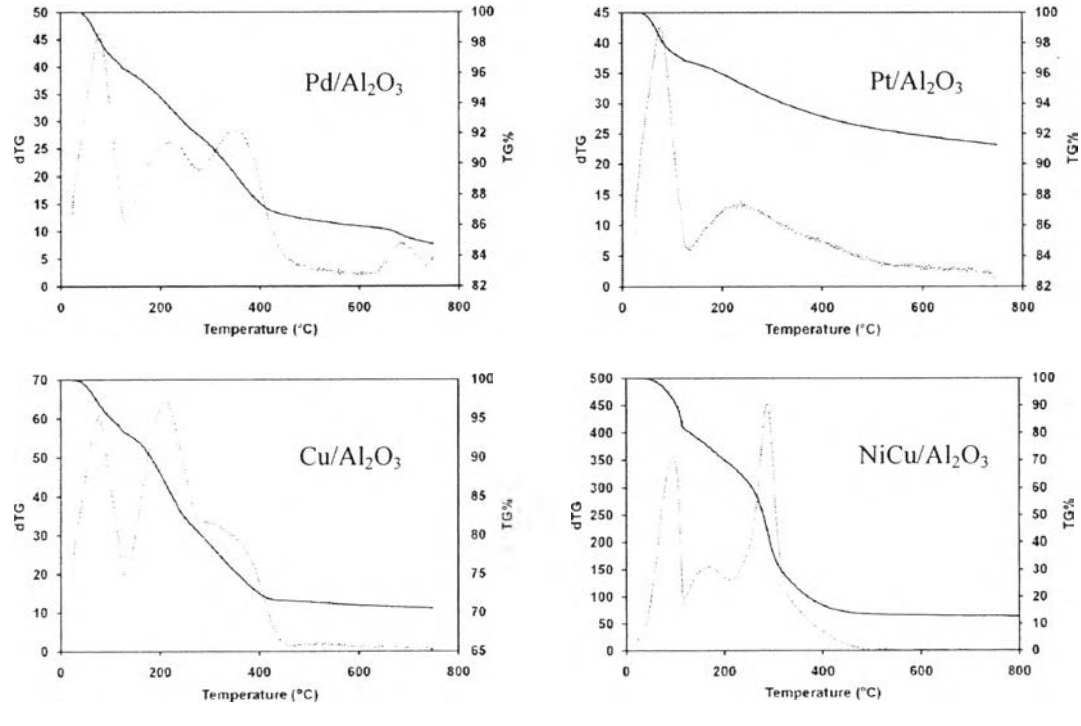

Figure 4.1 TGA profiles of prepared catalysts; dTG(····), TG(—).

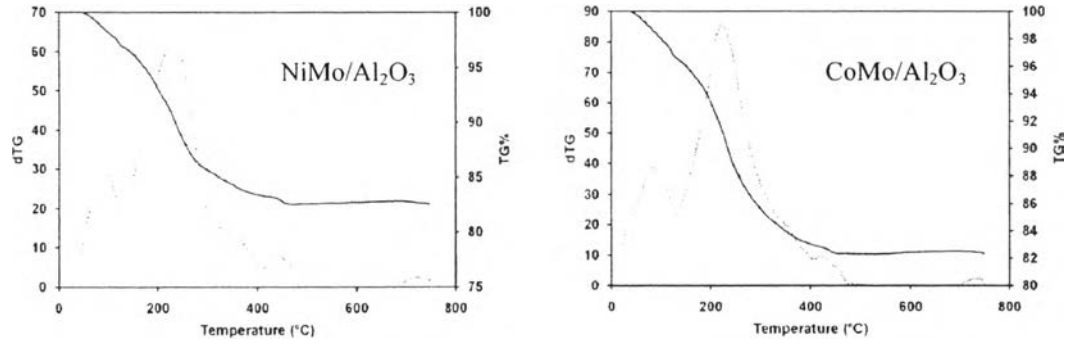

Figure 4.1 (cont.) TGA profiles of prepared catalysts; dTG(····), TG(—).

Table 4.1 The suitable calcination temperature of prepared catalysts

Catalyst	Calcination temperature (°C)
Pd/Al_2O_3	500
Pt/Al_2O_3	350
Cu/Al_2O_3	500
$NiCu/Al_2O_3$	500
$NiMo/Al_2O_3$	500
$CoMo/Al_2O_3$	500

4.1.2 Temperature Programmed Reduction (TPR)

Temperature programmed reduction was used to evaluate the suitable reduction temperature for each catalyst. The TPR profiles of Pd/Al_2O_3, Pt/Al_2O_3, Cu/Al_2O_3, $NiCu/Al_2O_3$, $NiMo/Al_2O_3$, and $CoMo/Al_2O_3$ catalysts are depicted in Figure 4.2 and the maximum temperatures (T_{max}) of H_2 consumption peak of these catalysts are listed in Table 4.2. The TPR profile of Pd/Al_2O_3 showed the negative peak at 103 °C. This peak is attributed to the decomposition of β-PdHx (Shekar *et al.*, 2005) which is formed by the reduction of palladium.

For Pt/Al_2O_3, the TPR pattern consisted of a small peak at 150 °C and two main reduction peaks at 257 and 413 °C. The small peak at low temperature was attributed to the reduction of PtO_2 species. The two peaks at 257 and 413 °C can be

assigned to oxychlorinated species in the bulk and two-dimensional phase, with a strong interaction with alumina, respectively (Navarro *et al*, 2005).

The TPR profile of Cu catalyst consisted of two peaks centered at 253 and 300 °C. The peak appeared at 253 °C was assigned to the reduction of Cu^{2+} species that were easily reduced. The high-temperature peak corresponded to the reduction of larger CuO particles which were less-reducible copper oxide (Lopez-Suarez *et al.*, 2008).

In the case of $NiCu/Al_2O_3$, two reduction peaks were observed at 242 and 437 °C. The low-temperature peak was assigned to a reduction of copper oxide and the peak at 437 °C belonged to a reduction of nickel oxide. The addition of Cu to Ni catalyst can lower the reduction temperature of nickel oxide. It can be suggested that the presence of metallic copper strongly promoted the nickel oxide reduction (De Rogatis *et al.*, 2009)

TPR profiles of $NiMo/Al_2O_3$, and $CoMo/Al_2O_3$ showed the main reduction peaks at 580 and 598 °C, respectively which represented the reduction of Mo species. The shoulder of TPR pattern of NiMo catalysts at 680 °C was associated with the reduction of Ni species, whereas a shoulder at 710 °C of CoMo catalyst can be assigned to the reduction of Co species (Betteridge and Burch, 1986). From TPR results, the suitable reduction temperatures for each catalyst are listed in Table 4.3.

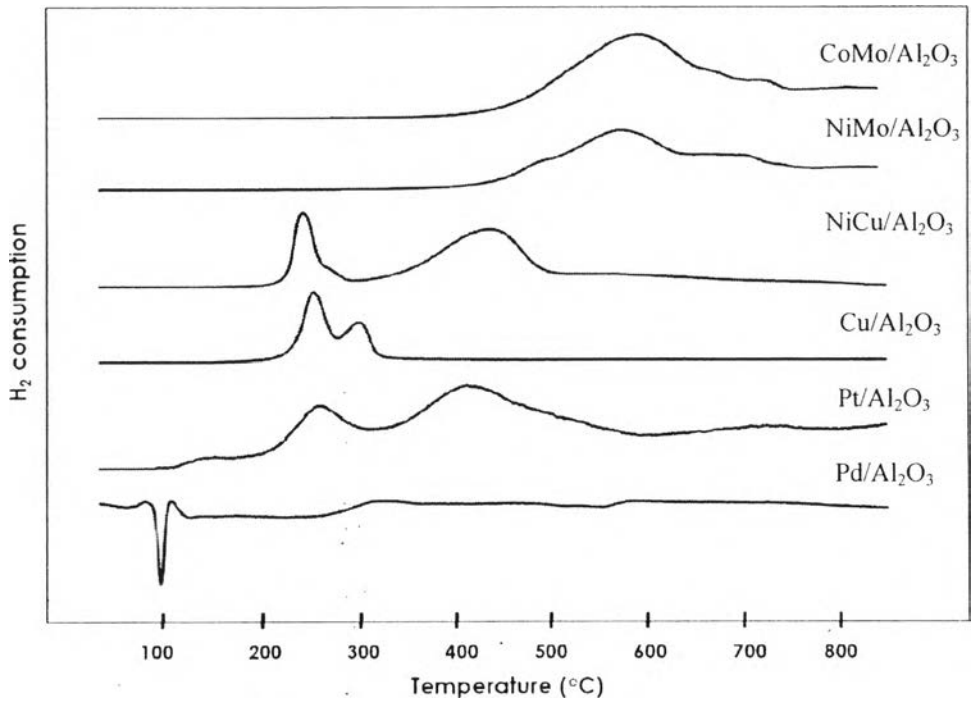

Figure 4.2 TPR profiles of the studied catalysts.

Table 4.2 TPR maximum temperatures (T_{max}) of H_2 consumption peaks of the studied catalysts

Catalyst	Low temperature peak T_{max} (°C)	High temperature peak T_{max} (°C)
Pd/Al_2O_3	103	-
Pt/Al_2O_3	257	413
Cu/Al_2O_3	253	300
$NiCu/Al_2O_3$	242	437
$NiMo/Al_2O_3$	-	580
$CoMo/Al_2O_3$	-	598

Table 4.3 The suitable reduction temperature for each catalyst

Catalyst	Reduction temperature (°C)
Pd/Al_2O_3	200
Pt/Al_2O_3	450
Cu/Al_2O_3	325
$NiCu/Al_2O_3$	425
$NiMo/Al_2O_3$	570
$CoMo/Al_2O_3$	580

4.1.3 X-ray Diffraction (XRD)

The XRD characterization was performed to identify unique metal oxide species of the studied catalysts. The XRD patterns of the catalysts were illustrated in Figure 4.3. The XRD patterns of Pd catalyst showed the diffraction signals at 2θ = 34°, 55°, 61°, and 71.5° which matched with the standard diffraction peaks of palladium oxide (PdO). There were no obvious Pt_2O as mentioned in TPR results due to the low Pd content (1 wt.%) and well-dispersed of Pt_2O on the γ-Al_2O_3. For Cu catalyst, the XRD pattern exhibited the signals at 2θ = 35.5°, 39°, 49°, 61.5°, and 68° which can be assigned to CuO species. This was in agreement with the TPR results which showed the present of CuO. In the case of NiCu catalyst, there were the signals of CuO same as Cu catalyst. The diffraction signals of NiO were observed at 2θ = 37°, 43°, 63°, and 79°. The distinct diffraction peaks of molybdenum oxide (MoO_3) were detected for both NiMo and CoMo catalysts. No obvious signals of nickel and cobalt oxide species were observed because of low metal loading of these species.

4.1.4 Brunauer-Emmett-Tellet Method (BET)

The BET surface area and pore volume of the catalysts are summarized in Table 4.4. Pt/Al_2O_3 catalyst shows the highest surface area of 262.2 m^2/g and a pore volume of 0.8753 cm^3/g corresponding to the lowest metal content. It can be indicated that the lower the metal loading, the higher the specific surface

area and pore volume of catalysts. However, $NiCu/Al_2O_3$ has BET surface area and pore volume higher than $NiMo/Al_2O_3$, and $CoMo/Al_2O_3$ which have lower metal loading.

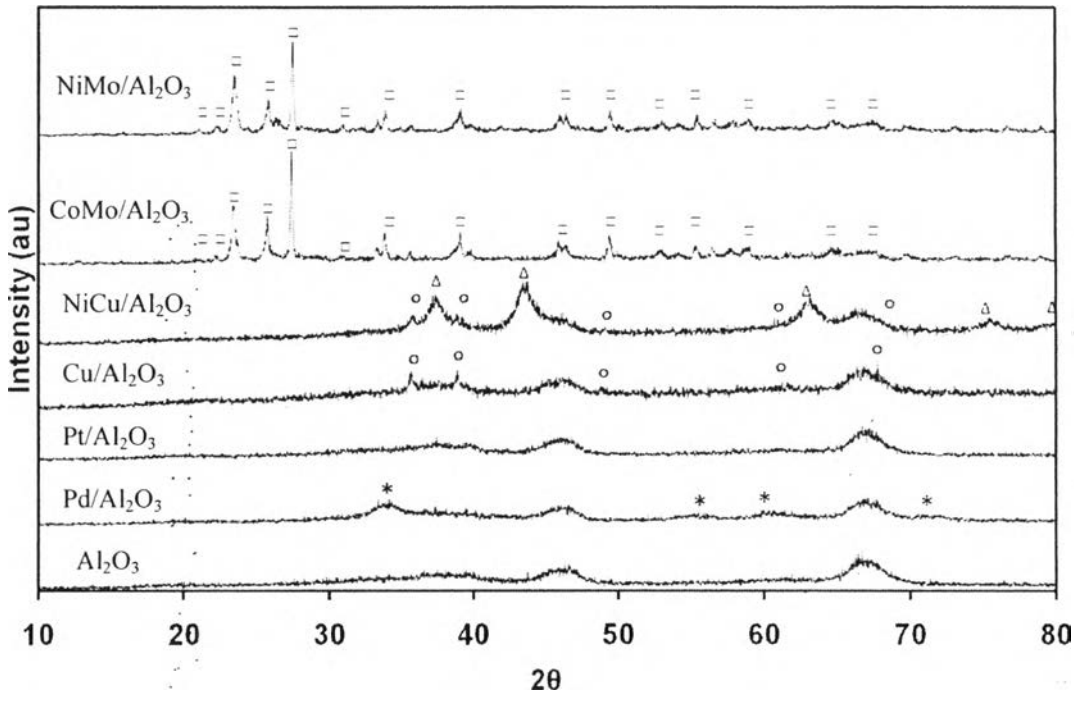

Figure 4.3 The XRD patterns of the studied catalysts. (*) PdO, (°) CuO, (Δ) NiO, (□) MoO_3.

Table 4.4 The textual properties of the studied catalysts

Catalyst	BET surface area (m^2/g)	Pore volume (cm^3/g)
Pd/Al_2O_3	222.5	0.7779
Pt/Al_2O_3	262.2	0.8753
Cu/Al_2O_3	217.1	0.7684
$NiCu/Al_2O_3$	144.9	0.4440
$NiMo/Al_2O_3$	108.8	0.3961
$CoMo/Al_2O_3$	99.2	0.3609

4.1.5 Temperature Program Oxidation (TPO)

The TPO profile and amount of coke deposited on the spent catalysts obtained after reaction over Pd/Al_2O_3, Pt/Al_2O_3, Cu/Al_2O_3, $NiCu/Al_2O_3$, $NiMo/Al_2O_3$, and $CoMo/Al_2O_3$ catalysts are illustrated in Figure 4.4 and Table 4.5, respectively. Pd, Pt, Cu, NiCu, NiMo, and CoMo catalysts exhibited main peaks at 370, 363, 338, 360, 343, and 344 °C, respectively. According to table 4.7, it showed that the amount of coke deposited on the spent catalysts increased in order Pt, NiCu, Pd, NiMo, CoMo, and Cu catalysts corresponding to the decreasing of the catalytic activity of these catalysts. The amount of coke deposited on Pt catalyst was relatively low corresponding to the highest activity of this catalyst.

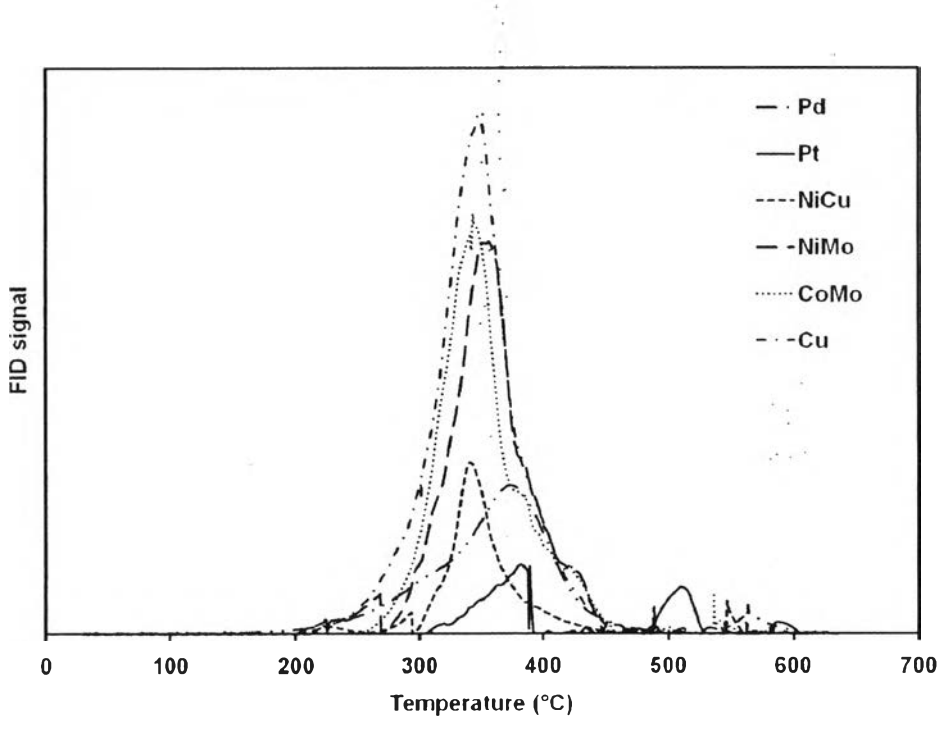

Figure 4.4 TPO Profile of the spent catalysts.

Table 4.5 Amount of carbon deposited on the spent catalysts

Catalysts	Pd	Pt	Cu	NiCu	NiMo	CoMo
wt.% C	19.22	5.36	41.60	9.76	31.76	33.17

4.2 Production of Hydrogenated Biodiesel from Jatropha Oil

4.2.1 Feed and Standard Analysis

The chromatogram of jatropha oil (10 wt.% crude jatropha oil in n-dodecane) analyzed by a GC/FID with cool-on column injector is shown in Figure 4.5. The chromatogram consists of two main peaks at 9 and 20 min which corresponding to n-dodecane (n-C12), and n-eicosane (n-C20) (internal standard), respectively. The peaks represent jatropha oil appears at 36-37 and 40-42 min which belong to diglycerides and triglycerides, respectively. The response factor value of jatropha oil is 1.0287.

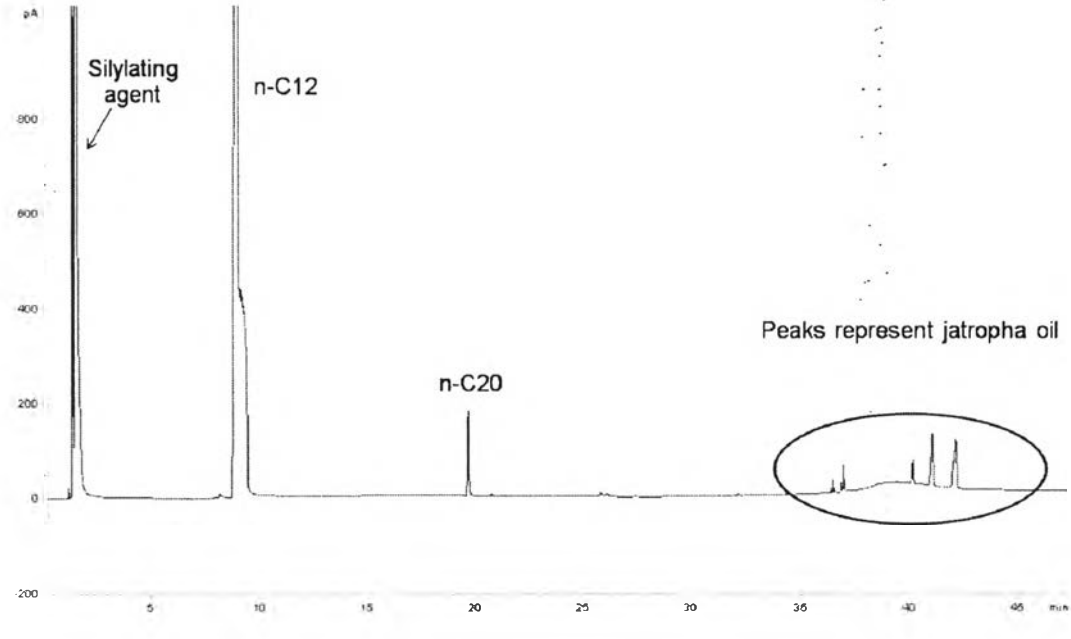

Figure 4.5 Chromatogram of 10 wt.% jatropha oil in n-dodecane.

The chromatograms of the mixture of standard chemicals are shown in Figure 4.6 and the retention times for each standard are listed in Table 4.6.

To find out the response factor of each standard chemical, the eicosane is used as the internal standard. The response factors of each substance in mixture of standard chemicals are also listed in Table 4.6.

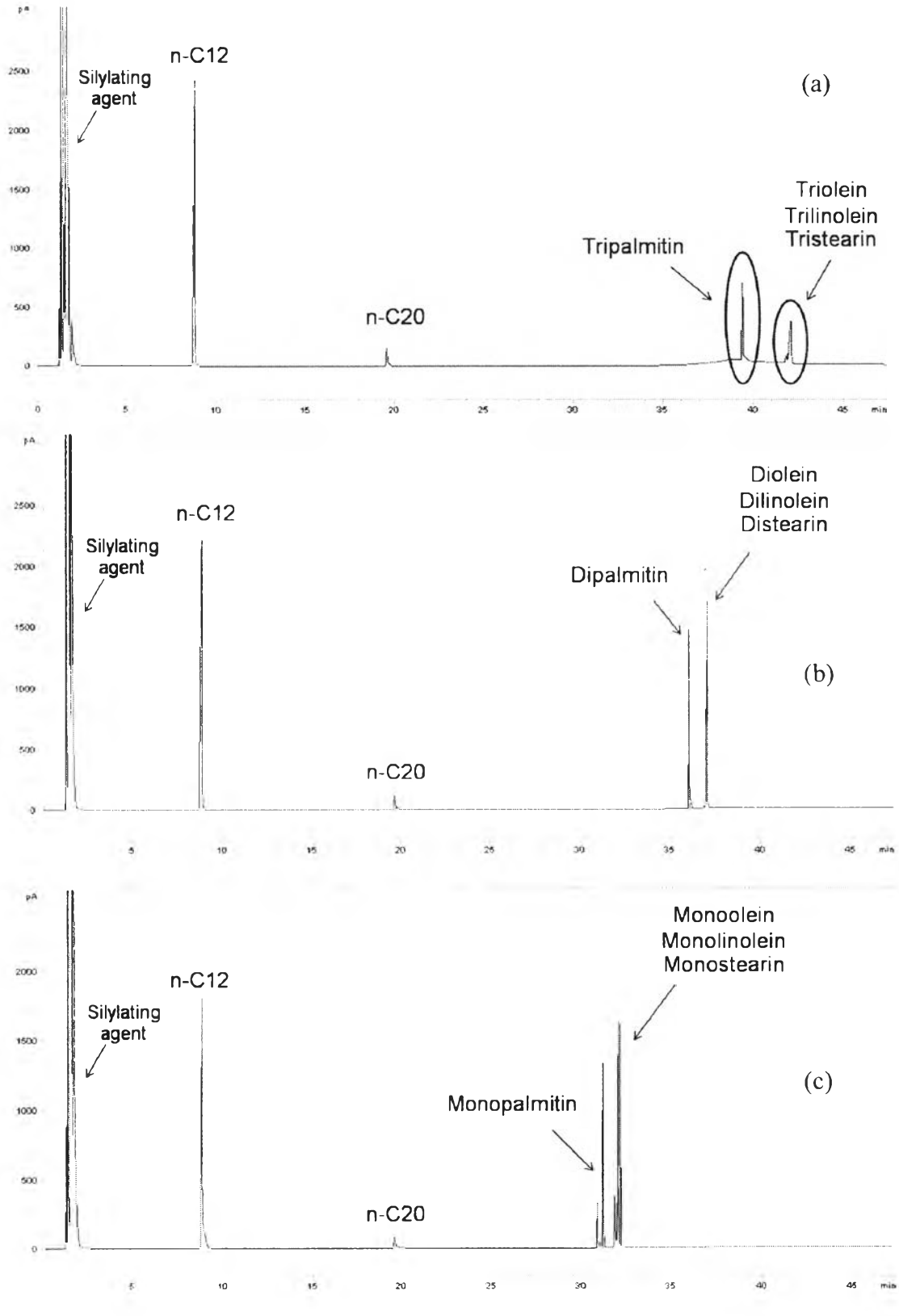

Figure 4.6 Chromatograms of standard chemicals, (a) triolein, trilinolein, tristearin, tripalmitin, (b) diolein, dilinolein, distearin, dipalmitin, (c) monoolein, monolinolein, monostearin, monopalmitin, (d) hexadecanol, octadecanol, palmitic acid, stearic acid, oleic acid (e) n-pentadecane, n-hexadecane, n-heptadecane, n-octadecane.

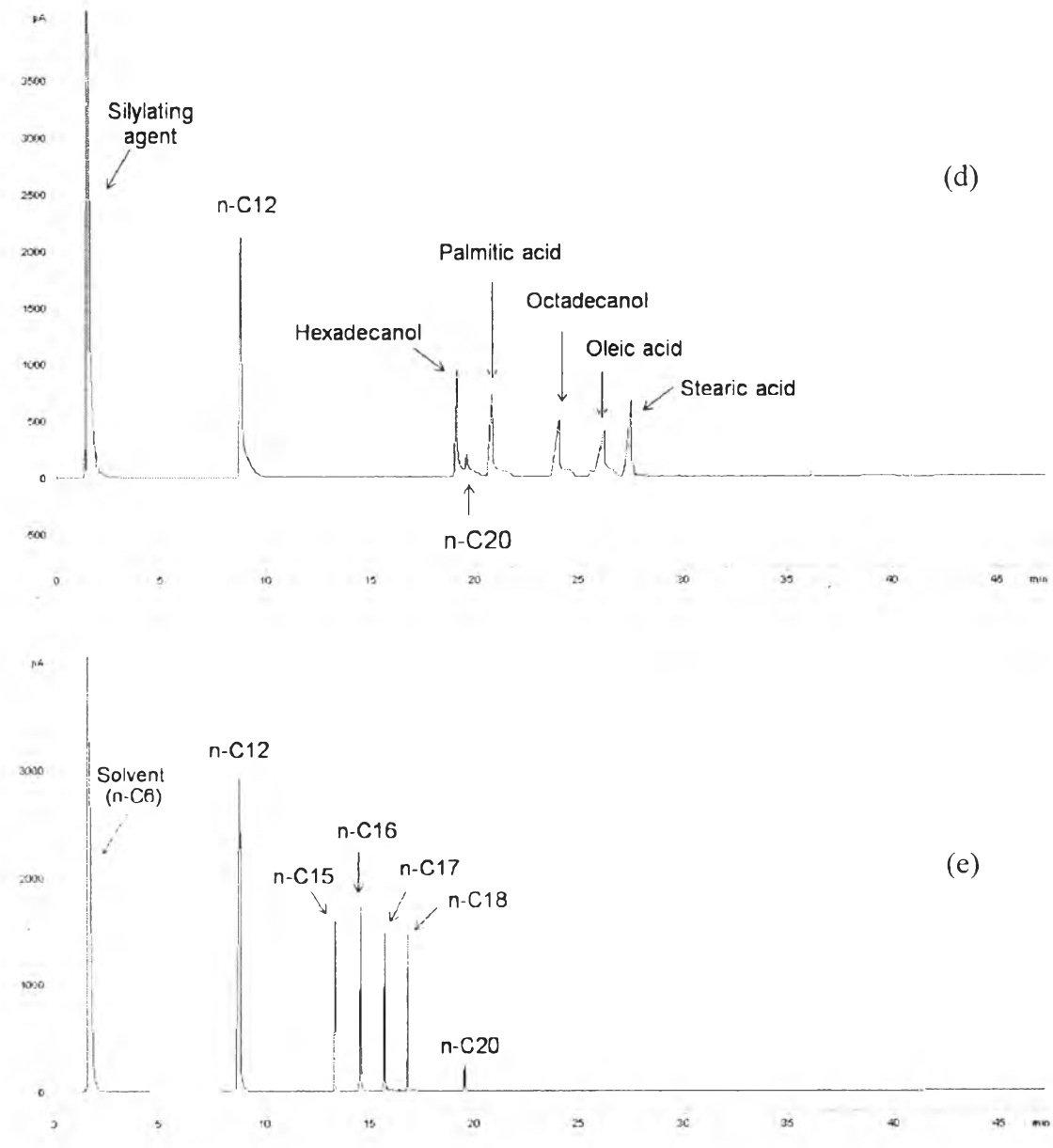

Figure 4.6 (cont.) Chromatograms of standard chemicals, (a) triolein, trilinolein, tristearin, tripalmitin, (b) diolein, dilinolein, distearin, dipalmitin, (c) monoolein, monolinolein, monostearin, monopalmitin, (d) hexadecanol, octadecanol, palmitic acid, stearic acid, oleic acid (e) n-pentadecane, n-hexadecane, n-heptadecane, n-octadecane.

Table 4.6 Retention times and response factors of standard chemicals

Standard chemicals	Retention times	Response factors
Triolein	42.1	0.9913
Trilinolein		
Tristearin		
Tripalmitin	39.4	1.0305
Diolein	37.0	0.9241
Dilinolein		
Distearin		
Dipalmitin	36.0	1.0166
Monoolein	32.2	1.6052
Monolinolein		
Monostearin		
Monopalmitin	31.3	1.5393
Hexadecanol	19.4	0.9994
Octadecanol	24.6	1.2587
Palmitic acid	20.8	1.1796
Stearic acid	27.8	0.9236
Oleic acid	26.1	0.9815
n-Pentadecane	13.5	1.3341
n-Hexadecane	14.8	1.2665
n-Heptadecane	15.9	1.2002
n-Octadecane	17.0	1.1795

The reference standards for gas product were analyzed by a Agilent-7890 equipped with thermal conductivity detector (TCD) with 80/100 Hyasep-Q column. Following the method for product analysis as described in Chapter III. The TCD signal of standard gases is shown in Figure 4.7. It was found that the retention time of carbon monoxide, carbon dioxide, methane, ethane, and propane are 0.76, 3.2, 1.68, 7.1, and 12.8, respectively.

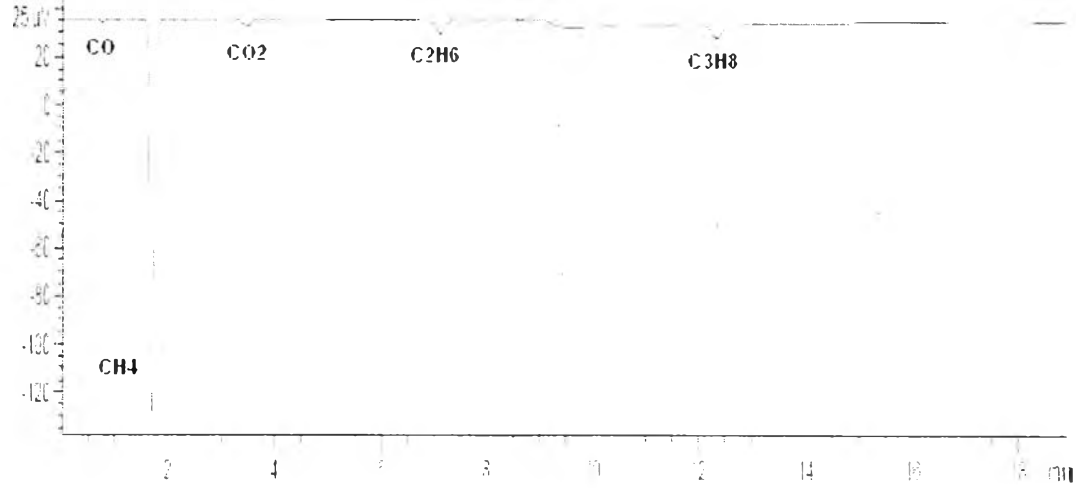

Figure 4.7 Chromatogram of the standard gases; CO, CO_2, CH_4, C_2H_6, and C_3H_8.

4.2.2 Conversion of Jatropha Oil

The deoxygenation of jatropha oil over Al_2O_3-supported catalysts with different active metals (Pd/Al_2O_3, Pt/Al_2O_3, Cu/Al_2O_3, $NiCu/Al_2O_3$, $NiMo/Al_2O_3$, and $CoMo/Al_2O_3$) was conducted at temperature of 325°C, reaction pressure of 500 psig, and H_2/feed molar ratio of 30 by varying liquid hourly space velocity (LHSV) from 0.5 to 4 h^{-1}. The typical chromatograms of a liquid product from the reaction over Cu/Al_2O_3 catalyst were shown in Figure 4.8. The first chromatogram (at LHSV 0.5 h^{-1}) consists of four main hydrocarbon peaks of n-pentadecane (n-C15), n-hexadecane (n-C16), n-heptadecane (n-C17), and n-octadecane (n-C18). Moreover, a small amount of octadecanol and stearic acid was detected. The second chromatogram (Figure 4.8B) shows the components of liquid-phase product obtained at LHSV 2 h^{-1}. Due to high LHSV (low contact time), the chromatogram is mainly

composed of feed remained and reaction intermediate peaks i.e. fatty alcohols, fatty acids, and fatty esters. The peaks representing hydrocarbons are relatively small.

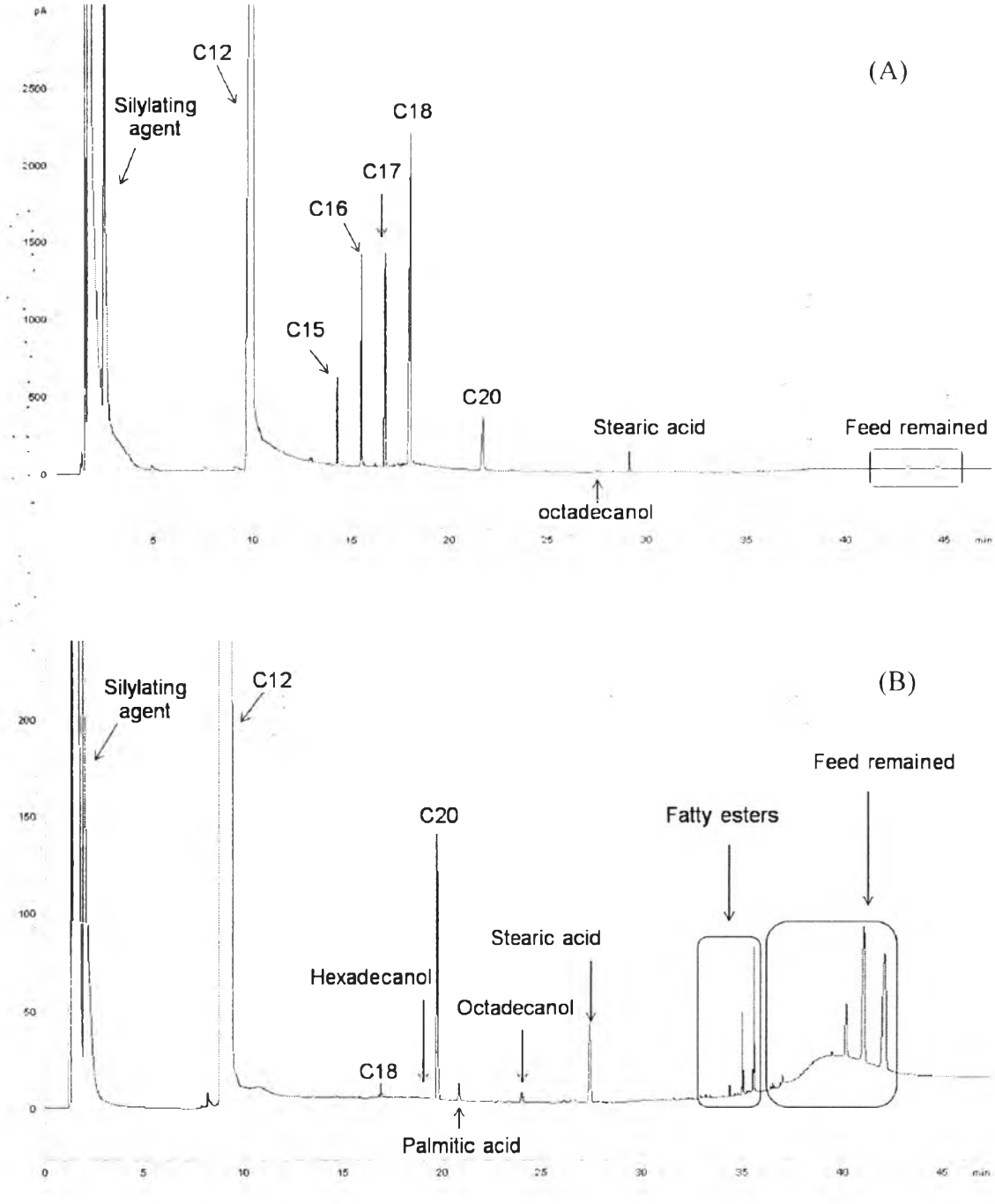

Figure 4.8 Chromatograms of liquid products at LHSV of (A) 0.5 h^{-1} and (B) 2 h^{-1} (catalyst: Cu/Al_2O_3, feed: CJO, reaction condition: temperature: 325 °C, pressure: 500 psig, H_2/feed molar ratio: 30. and TOS: 6 h).

In order to compare the catalytic activity or the performance of the studied catalysts, conversion of jatropha oil which mainly consists of triglyceride was determined. The conversion over the tested catalysts as a function of equivalent contact time (V/F) is shown in Figure 4.9. The solid points represent the conversion got from experimental data, whereas the solid lines are the conversion obtained by using the pseudo-first-order kinetics to fit the pertinent experimental data. It is seen that the experimental data followed the empiric pseudo-first-order-kinetics. From Figure 4.9, the conversion of jatropha oil from the reaction over the investigated catalysts is in the decending order Pt/Al_2O_3, $NiCu/Al_2O_3$, Pd/Al_2O_3, $NiMo/Al_2O_3$, $CoMo/Al_2O_3$, and Cu/Al_2O_3. Pt/Al_2O_3 catalyst achieved complete conversion of triglyceride at lower V/F (1 h) compared to the other catalysts. From these results, it can be suggested that the deoxygenation of triglycerides is irreversible reaction at the studied conditions that got complete conversion (Kubicka and Kaluza, 2010). The relative pseudo-first-order rate constants were calculated at the reaction temperature of 325 °C as shown in Table 4.7. The rate constants of conversion of triglycerides over different catalysts decrease in the same order as the conversion. The rate constant over Pt/Al_2O_3 is the highest which is higher than over NiCu, Pd, NiMo, CoMo, and Cu catalysts approximately 1.7, 2.6, 3.3, 3.9, and 6.2 times, respectively. According to the conversion and the rate constant, it can be concluded that Pt/Al_2O_3 catalyst has the highest activity for conversion of triglyceride-containing jatropha oil in comparison with the other five catalysts.

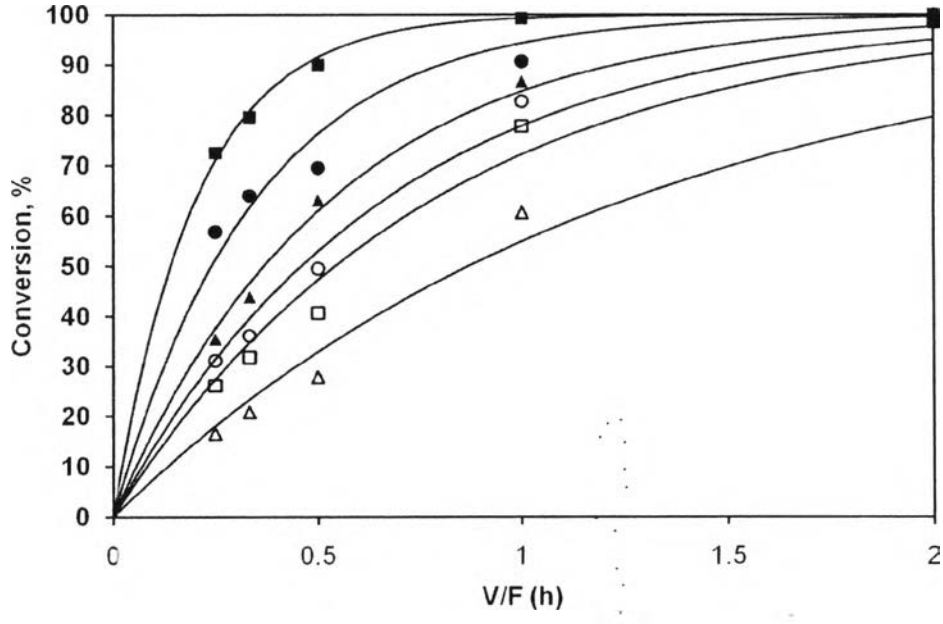

Figure 4.9 Conversion of jatropha oil over Pd (▲), Pt (■), Cu (△), NiCu (●), NiMo (○), and CoMo (□) catalysts. Solid points = experimental data, solid lines = conversion based on the pseudo-first-order kinetics approximation of experimental data.

Table 4.7 Relative pseudo-first order rate constants for triglycerides conversion at 325 °C

Catalyst	Relative pseudo-first order rate constant
Pd/Al_2O_3	1.88
Pt/Al_2O_3	4.94
Cu/Al_2O_3	0.80
$NiCu/Al_2O_3$	2.88
$NiMo/Al_2O_3$	1.51
$CoMo/Al_2O_3$	1.28

4.2.3 Overall Product Distribution

There are two main groups of liquid product obtained from deoxygenation reaction. The first group is hydrocarbons which mainly consist of n-pentadecane (n-C15), n-hexadecane (n-C16), n-heptadecane (n-C17), and n-octadecane (n-C18). The other group is oxygenates which are the reaction intermediates, i.e. fatty alcohols (hexadecanol and octadecanol), fatty acids (palmitic acid and stearic acids), fatty esters (palmitylpalmitate, palmitylstearate, stearylpalmitate, and stearylstearate), and small amount of monoglycerides. The selectivity to hydrocarbons and oxygenated based on the total yield of liquid product is depicted in Figure 4.10. The results show that the selectivity to hydrocarbons increased with increasing conversion, while the selectivity to oxygenates decreased with increasing conversion for all tested catalysts. According to the shape of the selectivity curves of hydrocarbons and oxygenates, it reveals that the hydrocarbons are the ultimate reaction products which are formed by the conversion of oxygenates. In addition, the selectivity to hydrocarbons of Pt/Al_2O_3 and $NiCu/Al_2O_3$ catalysts are higher than that of other catalysts corresponding to the lower selectivity to oxygenates. This can be indicated that catalytic deoxygenation activity of these two catalysts is higher than that of the other four catalysts. Pt/Al_2O_3 and $NiCu/Al_2O_3$ can convert the reaction intermediates into final hydrocarbon products faster than the others. Moreover, only small amount of isomerized hydrocarbons were detected, and no short chain liquid hydrocarbon were observed in this study.

Besides liquid products, water and gas products i.e. carbon oxide (carbon dioxide and carbon monoxide), methane, and propane were also detected. From both liquid and gas products, it can be seen that oxygen elimination from triglycerides proceed via the formation of water or carbon oxide. The formation of water corresponds to deoxygenation reaction carried out via hydrodexygenation pathway giving hydrocarbons with even number of carbon atoms in their molecules (corresponding to the number of carbon atoms of respective fatty acids bound in triglycerides) such as n-hexadecane and n-octadecane. On the other side, the formation of carbon dioxide and carbon monoxide relates to dacarboxylation and decarbonylation, respectively yielding hydrocarbons with odd number of carbon

atoms (one carbon atom less than in respective fatty acids) such as n-pentadecane and n-heptadecane.

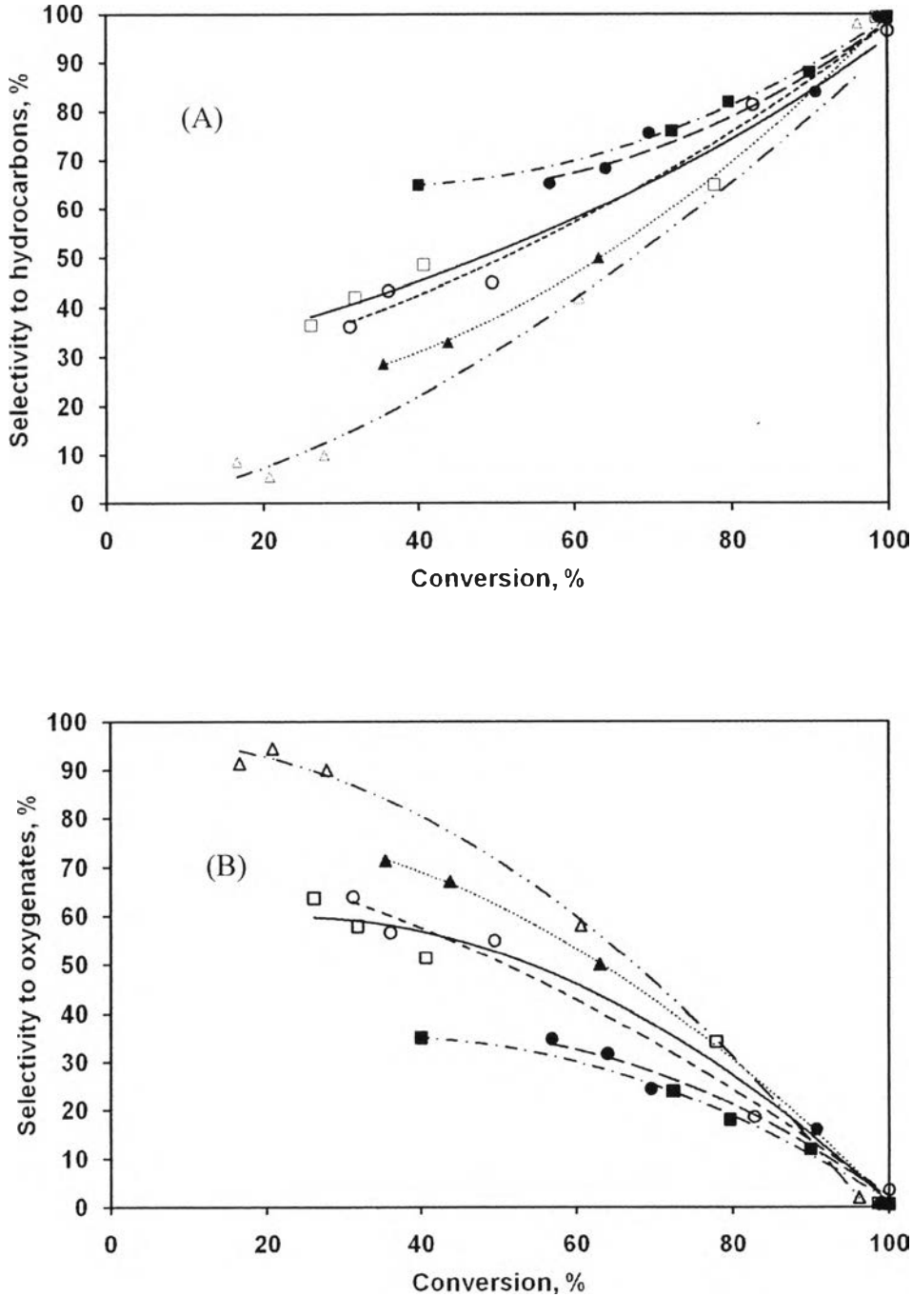

Figure 4.10 Selectivity to (A) hydrocarbons and (B) oxygenates as a function of conversion for Pd (▲), Pt (■), Cu (△), NiCu (●), NiMo (○), and CoMo (□) catalysts.

4.2.4 Product Distribution of Oxygenates

In order to understand clearly in the reaction mechanism of deoxygenation reaction, product distribution of oxygenate intermediates was investigated. Three main types of oxygenates were observed which are fatty acids (i.e. palmitic acid and stearic acid), fatty alcohol (i.e. hexadecanol and octadecanol), and fatty esters (i.e. palmitylpalmitate, palmitylstearate, stearylpalmitate, and stearylstearate). The fatty esters can be formed by esterification reaction between fatty acids and fatty alcohols under the experimental condition. The selectivity to each type of oxygenates is depicted in Figure 4.11. The inspection of Figure 4.11 A and B shows that the selectivity to fatty acids and fatty alcohols was high at low conversion and decreased with increasing conversion. This indicates that fatty acids and fatty alcohol were primary intermediates. Fatty acids are firstly formed by hydrogenolysis of triglycerides and further hydrogenation to generate fatty alcohols. The selectivity to fatty alcohols over Cu, NiMo, and CoMo catalyst are relatively higher than over Pd, Pt, and NiCu catalysts. It can be suggested that deoxygenation over Cu, NiMo, and CoMo catalysts preferably performs by hydrogenation fatty acids to form fatty alcohol and elimination oxygen by the formation of water, yielding final product, hydrocarbons (hydrodexygenation pathway). In contrast, the deoxyganation over the other three catalysts mainly proceeded via decarboxylation or decarbonylation pathways which do not generate fatty alcohols resulting in low selectivity to fatty alcohols. However, the selectivity to fatty alcohols over all catalysts was relatively low compared with fatty acids and fatty esters. It can be inferred that hydrogenation step of fatty alcohol occurs very rapidly.

From the selectivity curve of fatty esters (Figure 4.11 C), the fatty esters appeared corresponding to the decrease of fatty acids and fatty alcohols, and decreased at higher conversion. The evidence suggested that the fatty esters were not the prior intermediate and they were form by esterification of fatty acids and fatty alcohols. The selectivity to fatty ester over Cu, NiMo, and CoMo catalysts is significantly higher than over Pd, Pt, and NiCu catalysts because of low concentration of fatty alcohol formation over the latter three calalysts.

Interestingly, even at low triglyceride conversion, monoglycerides were observed in a trace amount, while diglycerides were not detected. This

observation suggested that the decomposition of a triglyceride to respective fatty acids occurred in one step.

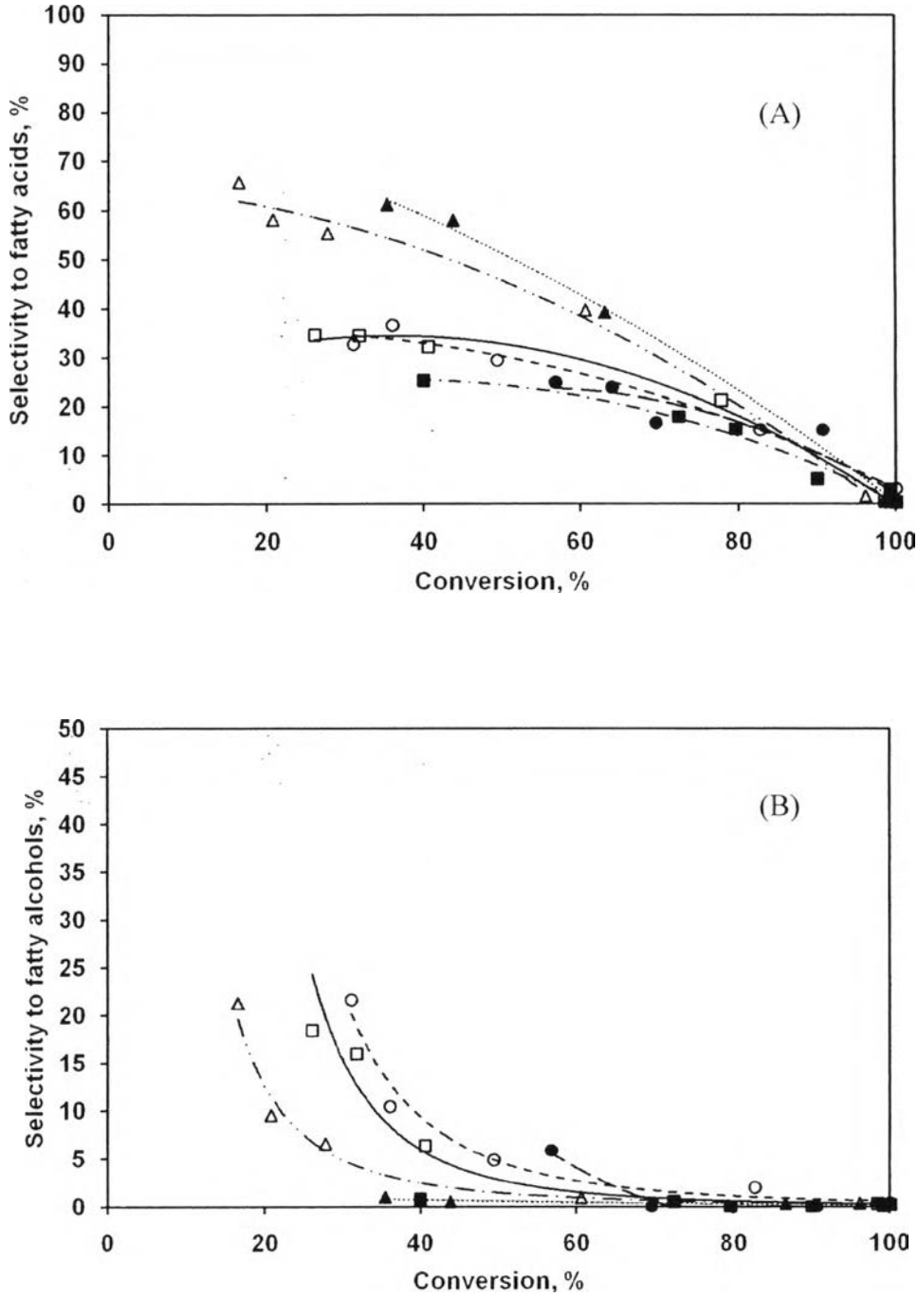

Figure 4.11 Selectivity to (A) fatty acids, (B) fatty alcohols, and (C) fatty esters as a function of conversion of triglycerides for Pd (▲), Pt (■), Cu (△), NiCu (●), NiMo (○), and CoMo (□) catalysts.

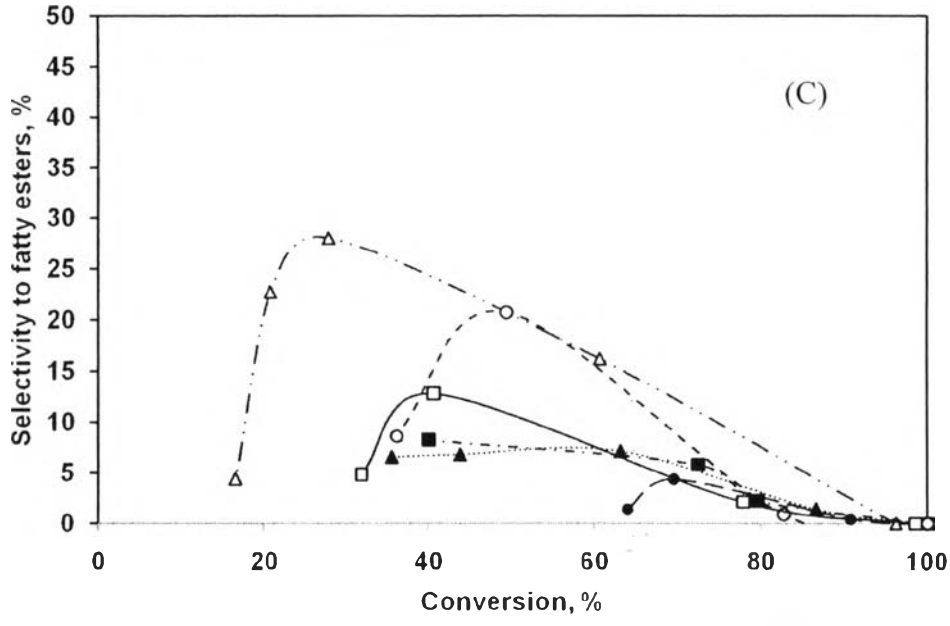

Figure 4.11 (cont.) Selectivity to (A) fatty acids, (B) fatty alcohols, and (C) fatty esters as a function of conversion of triglycerides for Pd (▲), Pt (■), Cu (△), NiCu (●), NiMo (○), and CoMo (□) catalysts.

4.2.5 Product Distribution of Liquid-phase Hydrocarbons

The selectivity to C16+C18 alkanes and C15+C17 alkanes (Figure 4.12) can be used as indicator to predict the reaction pathways of deoxygenation reaction. It gives important information about the final reaction step in deoxygenation. The results show that n-hexadecane and n-octadecane were formed selectively over Cu/Al_2O_3, $NiMo/Al_2O_3$, and $CoMo/Al_2O_3$ catalysts. It can be suggested that the deoxygenaton over these catalysts preferably proceeded via hydrodeoxygenation pathway which can be confirmed by water formation observed in the obtained liquid products. In contrast, n-pentadecane and n-heptadecane were formed mainly over Pt/Al_2O_3, Pd/Al_2O_3, and $NiCu/Al_2O_3$ catalysts corresponding to low selectivity to fatty alcohols (Figure 4.11 B). This can be inferred that decarboxylation and decarbonylation steps are faster than hydrodeoxygenation step. Furthermore, carbon oxide detected from gas analysis during the reaction indicates that deoxygenation over Pt/Al_2O_3, Pd/Al_2O_3, and $NiCu/Al_2O_3$ catalysts can be achieved mainly by decarboxylation and decarbonylation pathways.

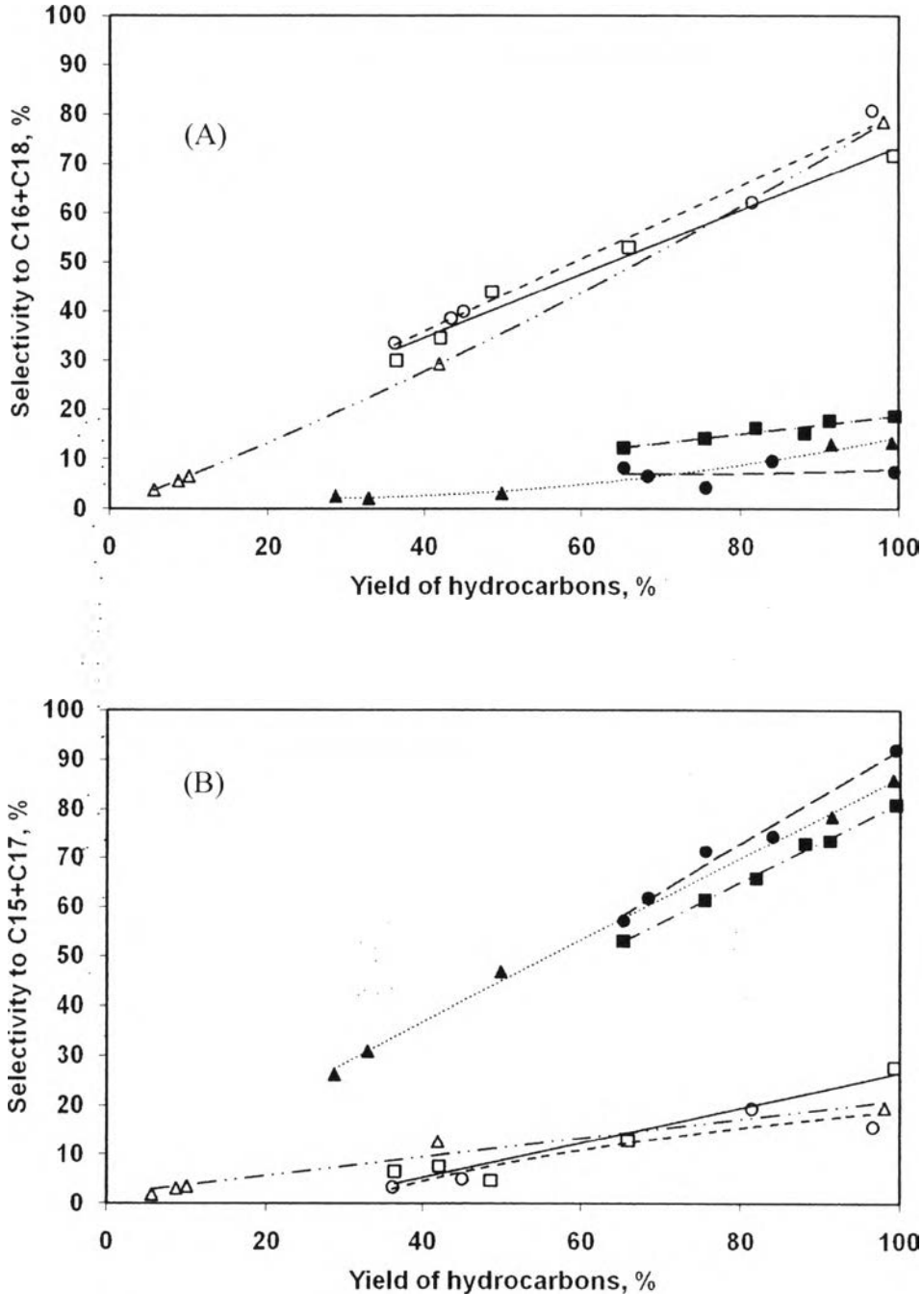

Figure 4.12 Selectivity to (A) n-hexatadecane and n-octadecane, and (B) n-pentadecane and n-heptadecane for Pd (▲), Pt (■), Cu (△), NiCu (●), NiMo (○), amd CoMo (□) catalysts.

4.2.6 Gas-phase Product Distribution

In addition to organic liquid products, gas products also were investigated by on-line GC equipped with thermal conductor detector (TCD). Gas analysis can provide additional information about reaction pathway over different catalysts so as to support the results from liquid product analysis. Gas products mainly consisted of carbon dioxide (CO_2), carbon monoxide (CO), propane, and methane. The concentrations of main gas products are illustrated in Figure 4.13. The inspection of Figure 4.13 reveals that the concentrations of carbon dioxide over Pd and NiCu catalysts were high while the highest concentration of carbon monoxide were observed over Pt catalyst. The difference in gas product distribution was reflected the different reaction mechanism. The evidence suggested that the deoxygenations of triglycerides over Pd and NiCu catalysts preferably carried out by removing oxygen as carbon dioxide whereas the deoxygenation over Pt catalyst mainly performed by the formation of carbon monoxide. It can be conclude that Pd and NiCu had high decarboxylation performance which this contrasts with Pt catalyst having high decarbonylation activity.

Furthermore, low concentrations of both carbon dioxide and carbon moxide over Cu, NiMo, and CoMo catalysts were examined since the deoxygenation over these catalysts did not preferably proceed via the two pathways mentioned above. They eliminated oxygen from triglyceride molecules as water observed in liquid product.

However, carbon dioxide reduction can take place to generate carbon monoxide and carbon monoxide methanation can also undergo resulting in methane formation. These reactions were undesired reactions since they caused significant amount of hydrogen consumption. From gas-phase product analysis, methane also was detected in gas components. Its concentration was relatively low compared with carbon oxide and propane (Figure 4.13 C). This suggested that methanation over the studied catalysts slightly occurred.

In addition, propane concentration corresponded to the conversion of triglycerides. So it can be employed as indicator of conversion value. The results show that propane concentration increased with increasing conversion.

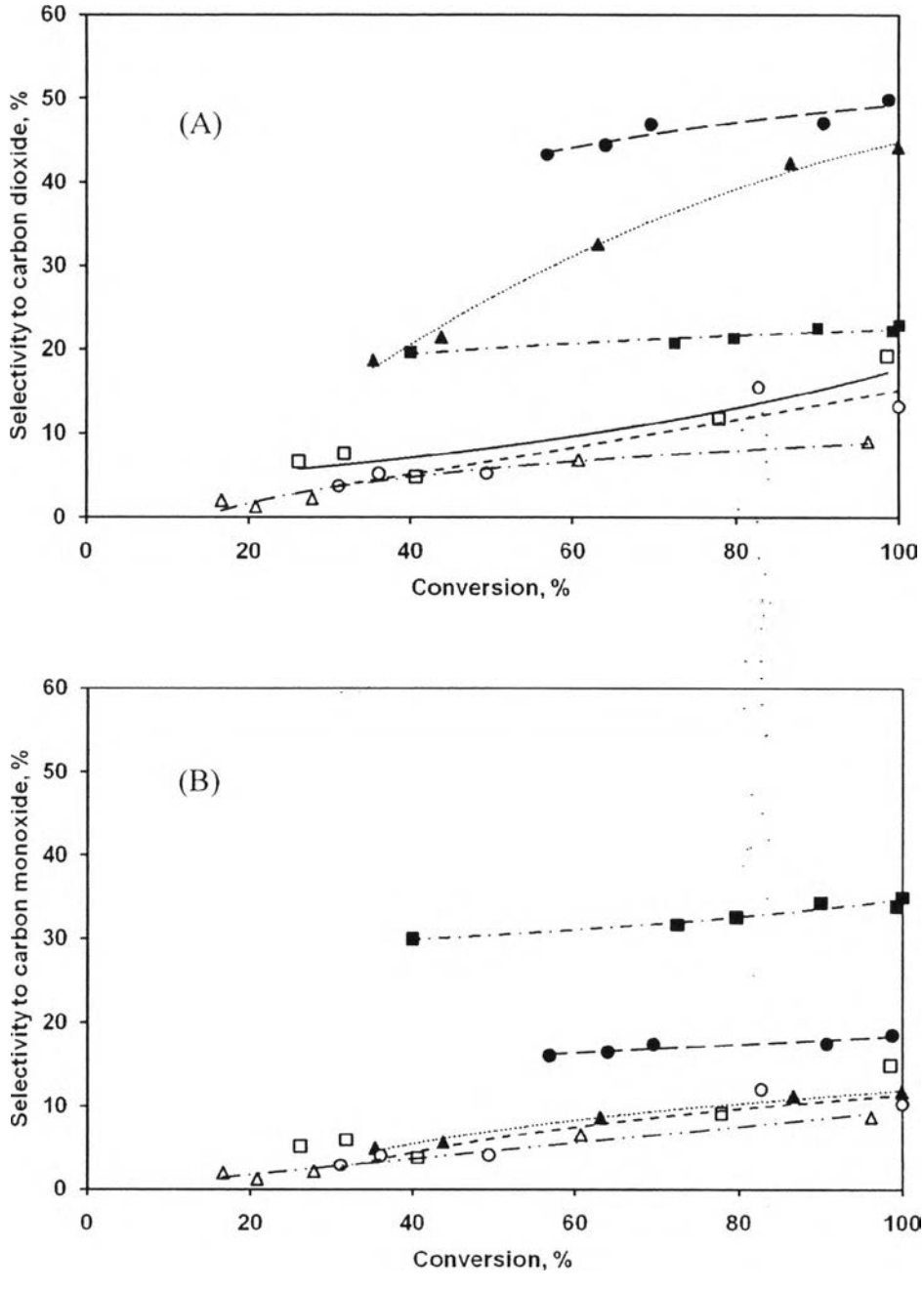

Figure 4.13 Concentrations of (A) carbon dioxide, (B) carbon monoxide, (C) methane, and (D) propane in hydrogen as a function of conversion for Pd (▲), Pt (■), Cu (△), NiCu (●), NiMo (○), amd CoMo (□) catalysts.

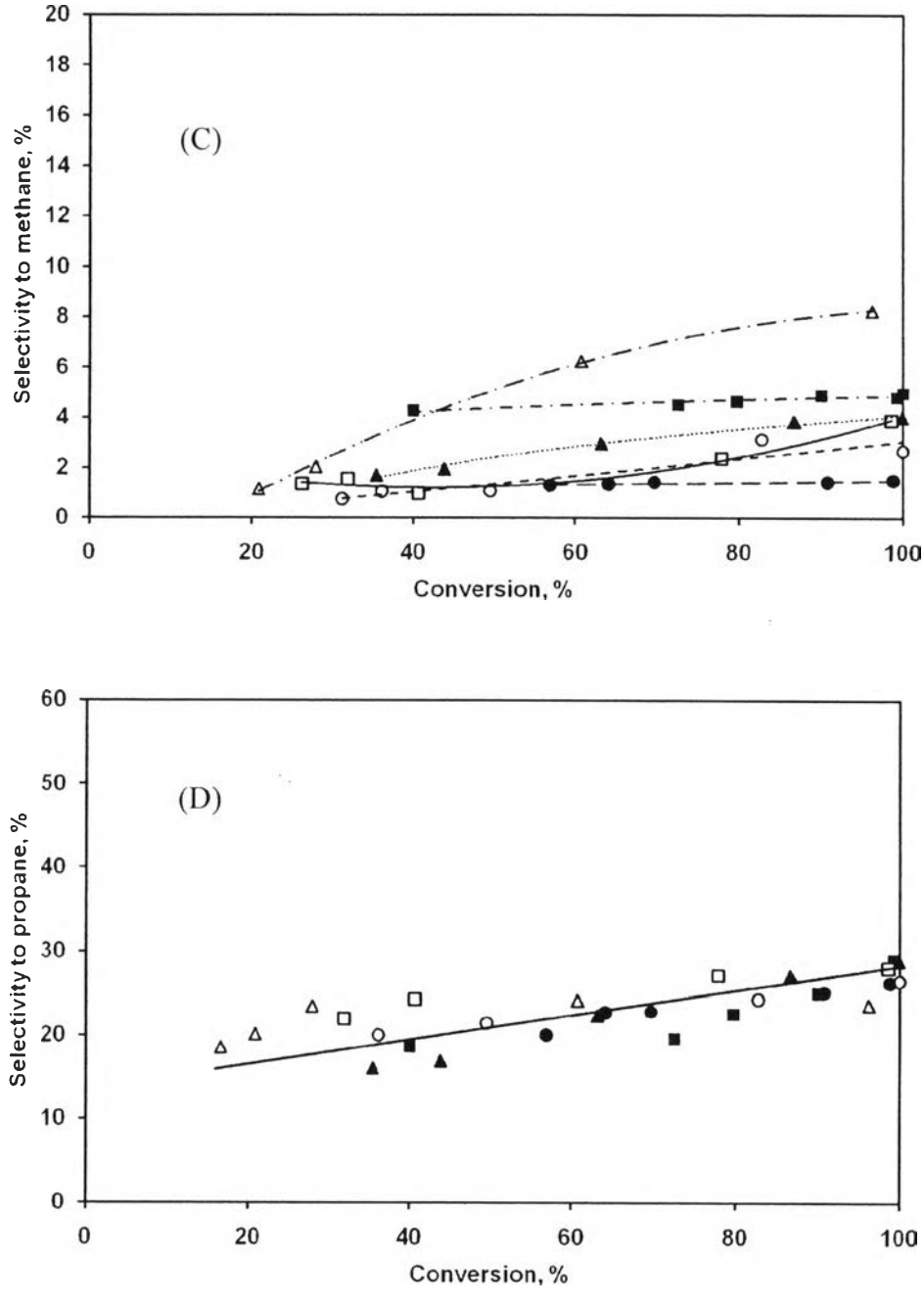

Figure 4.13 (cont.) Concentrations of (A) carbon dioxide, (B) carbon monoxide, (C) methane, and (D) propane in hydrogen as a function of conversion for Pd (▲), Pt (■), Cu (△), NiCu (●), NiMo (○), amd CoMo (□) catalysts.

4.2.7 Proposed Mechanism of Deoxygenation Reaction of Triglycerides

According to organic liquid and gas products analysis, the reaction mechanism of deoxygenation reaction can be proposed. The results showed that deoxygenation reaction proceeded in consecutive steps. First of all, unsaturated triglycerides in jatropha oil were hydrogenated into hydrogenated triglyceride. Then they were further hydrogenated and broken down into fatty acids. After that, fatty acids can undergo three main reaction pathways: decarboxylation, decarbonylation and hydrodeoxygenation. The first pathway (i), fatty acids were decarboxylated to alkane products that have one carbon atom less than the original fatty acids in each oil molecule (n-pentadecane (n-C15) and n-heptadecane (n-C17)) having CO_2 as a by-product. This path is called decarboxylation. The second patyway (ii), decarbonylation, fatty acids were decarbonylated and further hydrogenated to alkane products with same carbon numbers as decarboxylation having CO and H_2O as a by-product. The last pathway (iii), carbonyl groups of fatty acids were hydrogenated into fatty alcohols, followed by dehydration and hydrogenation of fatty alcohols to long chain alkanes with carbon atoms equivalent to the carbon atoms of fatty acids in each oil molecule (n-hexadecane (n-C16) and n-octadecane (n-C18)) having H_2O as by product. This pathway is called hydrodeoxygenation. Since there were fatty acids and fatty alcohols formed in this pathway, so they can undergo esterification reaction yielding fatty esters.

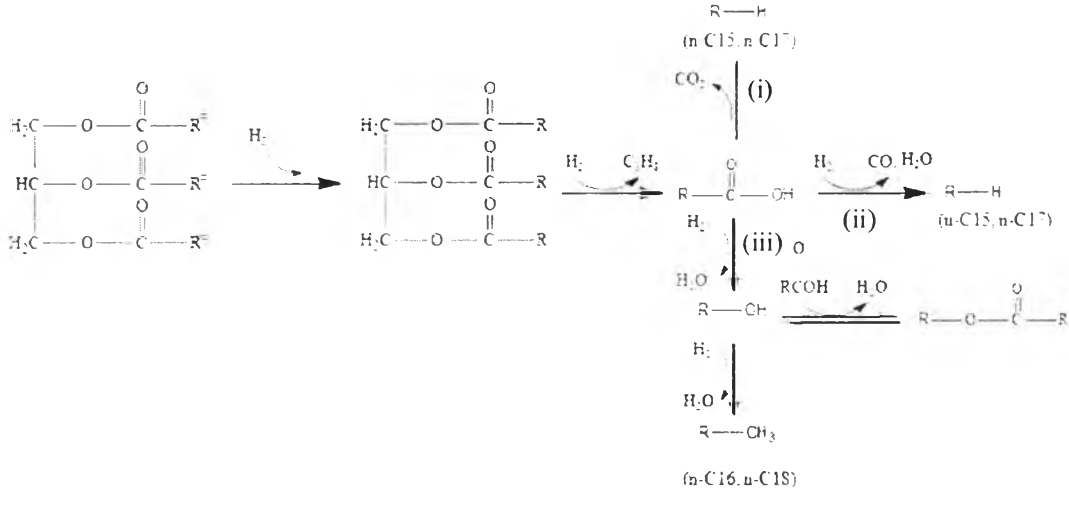

Figure 4.14 Proposed reaction pathways for the deoxygenation of vegetable oils under H_2 atmosphere.

4.2.8 Stability Testing of Pt/Al_2O_3 and $NiCu/Al_2O_3$ on the Deoxygenation of Jatropha Oil

The Pt/Al_2O_3 and $NiCu/Al_2O_3$ catalysts were selected to test for its stability in the deoxygenation of jatropha oil for 1 week. The results are shown in Figure 4.15, the jatropha oil conversion over Pt/Al_2O_3 slightly decreased with time on stream compared with $NiCu/Al_2O_3$ catalyst. It can be concluded that Pt/Al_2O_3 catalyst had better catalytic stability than $NiCu/Al_2O_3$ catalyst. n-C15 and n-C17 are favorable to be produced compared to n-C16 and n-C18 over both catalysts. The amount of intermediate products increased with time on stream whereas hydrocarbons decreased with time on stream due to the catalyst deactivation.

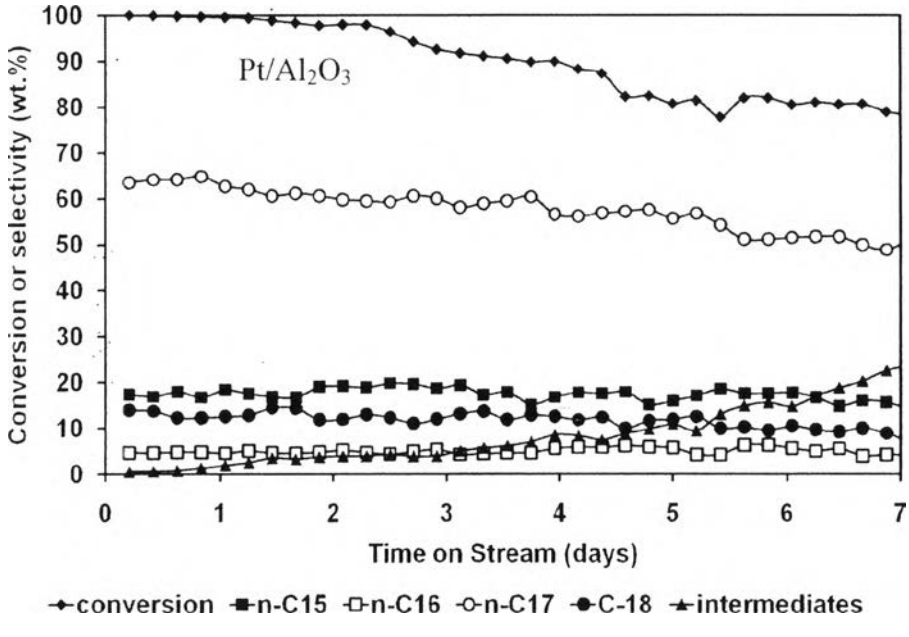

Figure 4.15 Long term stability testing of the Pt/Al_2O_3 and $NiCu/Al_2O_3$ catalysts on the deoxygenation of jatropha oil.

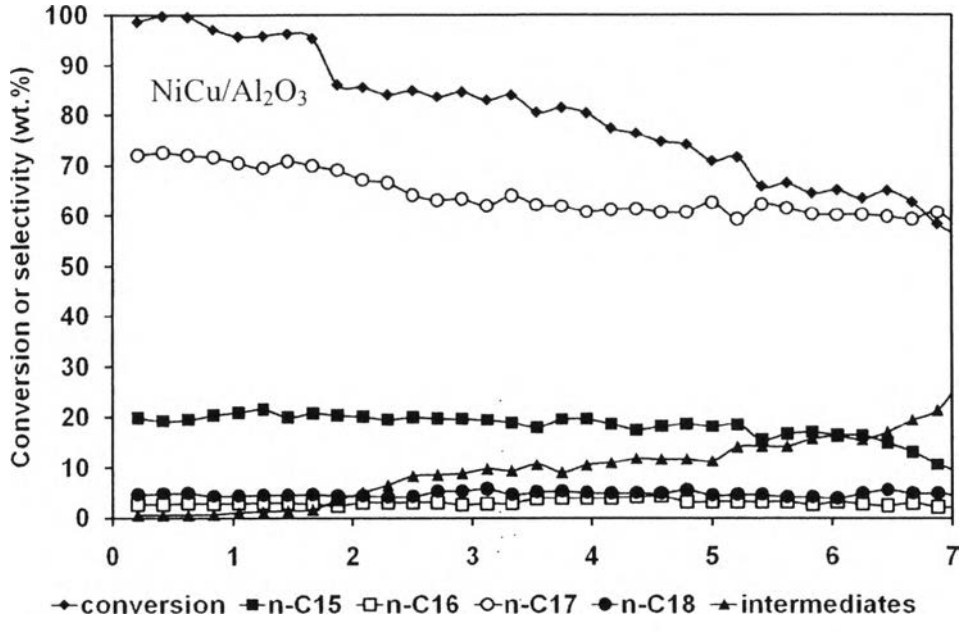

Figure 4.15 (cont.) Long term stability testing of the Pt/Al_2O_3 and $NiCu/Al_2O_3$ catalysts on the deoxygenation of jatropha oil.